

Parameter Optimisation of a H-type Three-blade Contra-rotating Vertical-axis Wind Turbine at Low Tip-speed Ratio

Z. Zhao, K. Chen[†], Q. Wang, T. Su and H. Hu

College of Mechanical Engineering, Xinjiang University, Urumqi 830046, China

[†]Corresponding Author Email: chenkun@xju.edu.cn

ABSTRACT

Renewable energy sources such as wind energy can alleviate climate deterioration and the global energy crisis, and a major piece of equipment for capturing wind energy is the vertical-axis wind turbine (VAWT), with contra-rotating VAWTs (CR-VAWTs) having received focused attention because of their excellent stability. In the study reported here, Taguchi's method and computational fluid dynamics were used to optimise the four main parameters in the configuration of a three-blade H-type CR-VAWT, i.e. rotor spacing (S), diameter-to-height ratio (D/H), phase angle (α), and rotational direction (r). The optimum CR-VAWT was derived, and its power coefficients were compared with those of a stand-alone VAWT under low tip-speed ratio (TSR). It was found that D/H has the most effect (81.21%) on the CR-VAWT power performance, followed by α (7.37%) and then r (5.83%), with S having the least effect (5.59%). Compared to the stand-alone VAWT, the average power coefficient of the optimum CR-VAWT is much smaller when the TSR is less than 1.25, but the power performance of the latter gradually prevails as the TSR increases. At a TSR of 1.6, the optimum CR-VAWT has an average power factor improvement of 10.6% over the stand-alone VAWT. At the same time, the maximum total torque of the optimum CR-VAWT is only 6% of that of the stand-alone VAWT, giving the CR-VAWT good stability.

Article History

Received October 10, 2024

Revised January 14, 2025

Accepted January 20, 2025

Available online March 30, 2025

Keywords:

*Contra-rotating vertical axis
wind turbine (CR-VAWT)*

Taguchi's method

Parameter optimisation

Low tip-speed ratio

Power performance

1. INTRODUCTION

In recent years, global climate deterioration and resource poverty have become two serious challenges facing human society (Peng et al., 2021). While traditional energy sources cause environmental pollution and energy shortages, wind energy has the benefits of abundant resources and wide distribution (Dong et al., 2022). Among the main devices for utilising wind energy are wind turbines, which can be categorised into horizontal-axis wind turbines (HAWTs) and vertical-axis wind turbines (VAWTs). VAWTs have many advantages over HAWTs, such as low noise, no need for a yawing device, simple structure and stable operation in any wind direction (Wang et al., 2018). Therefore, VAWTs are the best choice for future applications in rural, urban and offshore scenarios.

Based on their operating principle, VAWTs can be classified into lifting ones (e.g. the Darrieus model) and dragging ones (e.g. the Savonius model). Darrieus wind turbines are driven by aerofoil-generated lift, and compared with Savonius wind turbines, they produce

greater torque at higher wind speeds and have higher wind energy utilisation (Li et al., 2023), thereby attracting global research attention.

Many scholars have worked to enhance the aerodynamic efficiency of VAWTs, and Table 1 summarises that research. Via wind-tunnel testing, Sun et al. (2023) researched how the pitch angle and aerofoil cross-section affect the aerodynamic efficiency of wind turbines; their findings showed that the power coefficient of wind turbines whose blades use the NACA0018 aerofoil increases under high tip-speed ratio (TSR) and decreases under excessively large pitch angle. Using computational fluid dynamics (CFD), Zhang et al. (2020) explored how the aerofoil thickness affects the aerodynamic efficiency of NACA four-digit aerofoils, and they found that straight blades with symmetrical aerofoils have the best dynamic efficiency. Lee and Lim (2015) used CFD to study the impact of wind-turbine parameters on energy utilisation; they showed that at low TSR, the wind energy utilisation of wind turbines increases with increasing chord length and decreasing wind-turbine diameter.

Table 1 Summary of recent research on vertical-axis wind turbines (VAWTs)

Authors	Method	Research content and key findings
Sun et al. (2023)	Wind-tunnel tests	Researched how pitch angle and aerofoil cross-section affect the aerodynamic efficiency of wind turbines. The findings showed that the power coefficient of wind turbines whose blades use the NACA0018 aerofoil increases under high TSR and decreases under excessively large pitch angle.
Zhang et al. (2020)	CFD	Explored how aerofoil thickness affects the aerodynamic efficiency of NACA four-digit aerofoils and found that straight blades with symmetrical aerofoils give the best dynamic efficiency.
Lee and Lim (2015)	CFD	Studied how wind-turbine parameters affect energy utilisation. They showed that at low TSR, the wind energy utilisation of wind turbines increases with increasing chord length and decreasing wind-turbine diameter.
Farzadi and Bazargan (2023)	CFD	Investigated the properties of J-type blades in various operating situations and found that they produce more torque and provide improved self-starting performance, particularly at low wind speed.
Zhu et al. (2021)	CFD	Explored how the geometric parameters of Gurney flaps affect the performance of VAWTs with straight blades. The findings showed that the best aerodynamic performance enhancement for straight blades is when the flap length is 0.75% and the width is 0.12% of the chord length.
Zhang et al. (2022)	CFD	Examined the spreading speed and vortex characteristics of VAWTs with bionic and prototype blades and found that the former inhibit the tip-vortex effect on the cross-section speed and have slightly better aerodynamic performance compared to the latter.
Malicki et al. (2024)	CFD	Presented a new drag-driven VAWT and used CFD to optimise the wind-turbine diameter, number of blades, shape and cavity depth parameters. The outcomes indicated that a five-blade rotor operates with the maximum efficiency and a higher average torque coefficient when the palisade spacing is 10–20 mm.
Didane et al. (2018, 2019)	CFD and wind-tunnel tests	Created a novel CR-VAWT model and used CFD and wind-tunnel testing to analyse it, showing a threefold improvement in power performance.
Poguluri et al. (2021)	CFD	Investigated the aerodynamic efficiency of a CR-VAWT, which showed a slight decrease in efficiency compared to a stand-alone VAWT, mainly because of the significant interaction between the vortices at the top and bottom rotor tips.
Zheng et al. (2024)	CFD and response surface optimisation	Carried out simulations of the proposed CR-VAWT and showed that its energy utilisation was less than that of a stand-alone VAWT. However, the torques generated by the top and bottom rotors on the base cancelled each other for better stability.
Sanaye and Farvizi (2024)	CFD and Taguchi's method	Optimised the parameters of a helical VAWT to increase its aerodynamic efficiency considerably.
Hassanpour and Azadani (2021)	CFD and Taguchi's method	Optimised the layout parameters of a pair of VAWTs arranged side by side. The outcomes indicated that the wind energy utilisation of the optimally laid out pair of VAWTs was improved by 26.6% compared to a stand-alone VAWT.
Radhakrishnan et al. (2023)	CFD and Taguchi's method	Optimised the parameters of a CR-VAWT and obtained the optimum one with better power performance than a stand-alone VAWT over the entire TSR range.

Many researchers have also enhanced the aerodynamic performance of VAWTs via aerofoil improvement. [Farzadi and Bazargan \(2023\)](#) used CFD to investigate the properties of J-type blades in various operating situations, and they found that J-type blades produce more torque and provide improved self-starting performance, particularly at low wind speed. [Zhu et al. \(2021\)](#) used CFD to explore how the geometrical parameters of Gurney flaps affect the performance of VAWTs with straight blades; the findings showed that the best aerodynamic performance enhancement for straight

blades is when the flap length is 0.75% and the width is 0.12% of the chord length. [Zhang et al. \(2022\)](#) used CFD to examine the spreading speed and vortex characteristics of VAWTs with bionic and prototype blades and found that the former inhibit the tip-vortex effect on the cross-section speed and have slightly better aerodynamic performance compared to the latter. [Malicki et al. \(2024\)](#) presented a new drag-driven VAWT and used CFD to optimise the wind-turbine diameter, number of blades, shape and cavity depth parameters; the outcomes indicated that a five-blade rotor operates with the maximum

efficiency and a higher average torque coefficient when the palisade spacing is 10–20 mm.

In addition, there is now much research interest in counter-rotating VAWTs (CR-VAWTs), which comprise two rotors revolving around a common vertical axis in opposite directions. By enclosing an S-type rotor inside an H-type rotor, [Didane et al. \(2018, 2019\)](#) created a novel CR-VAWT, and they analysed it using CFD and wind-tunnel testing; the outcomes indicated a threefold improvement in the power performance of the new model. [Poguluri et al. \(2021\)](#) used CFD to investigate the aerodynamic efficiency of a CR-VAWT, which showed a slightly decrease in efficiency compared to a stand-alone VAWT; the main reason for this is the significant interaction between the vortices at the top and bottom rotor tips. [Zheng et al. \(2024\)](#) combined CFD with response surface optimisation to carry out a simulation study of the proposed CR-VAWT; they showed that the energy utilisation of the CR-VAWT was less than that of a stand-alone VAWT, but the torques generated by the top and bottom rotors on the base cancelled each other for better stability.

Taguchi's method is an effective multifactor method for quality optimisation ([Liao & Kao, 2010](#)), and it can be used to optimise the parameters affecting wind-turbine performance ([Chen et al., 2017](#)). [Sanaye and Farvizi \(2024\)](#) used CFD and Taguchi's method to optimise the parameters of a helical VAWT; the outcomes suggested considerably increased aerodynamic efficiency of the optimum helical VAWT. [Hassanpour and Azadani \(2021\)](#) used Taguchi's method to optimise the layout parameters of a pair of VAWTs arranged side by side; the outcomes indicated that the wind energy utilisation of the optimally laid out pair of VAWTs was improved by 26.6% compared to a stand-alone VAWT. [Radhakrishnan et al. \(2023\)](#) used a combination of CFD and Taguchi's method to optimise the parameters of a CR-VAWT, and they arrived at the optimum CR-VAWT with better power performance than a stand-alone VAWT in the entire TSR range.

However, despite the many simulation and experimental studies of VAWTs, there have been relatively few involving the design and simulation of CR-VAWTs. In particular, there has been insufficient study of how the direction of rotation between the top and bottom rotors and the phase angle between the rotors affect the aerodynamic efficiency of a three-blade H-type CR-VAWT. Therefore, herein the four main parameters affecting the power performance of a CR-VAWT are selected for three-dimensional simulation and then analysed, i.e. rotor spacing (S), diameter-to-height ratio (D/H), phase angle (α) and rotational direction (r). A four-factor L16 mixed orthogonal table is established to identify the optimum CR-VAWT via orthogonal experiments and to reveal the effect degree of each factor on the CR-VAWT aerodynamic efficiency. Meanwhile, the power performance of the optimum CR-VAWT is compared with that of a stand-alone VAWT at a low TSR, and the mechanism is analysed and investigated via the pressure field.

2. METHODOLOGY

2.1 Geometric Modelling

Herein, a three-blade compact H-VAWT is chosen for study. Figure 1 shows the structural brief of the CR-VAWT, which consists of two rotors; the top and bottom rotors revolve in opposite directions, with a disk generator connected to the middle and a base support at the bottom. Figure 2 and Table 2 specify the detailed parameters of the CR-VAWT. The calculation model used herein simplifies the rotating shaft, connecting rod, disk generator and base support in Fig. 1. NACA0021 is selected as the reference aerofoil type, with aerofoil chord length $c = 0.2$ m, wind-turbine diameter $D = 0.6$ m and height $H = 0.8$ m. The initial spacing is $S = 0.25H = 0.2$ m. The rotational directions of the top and bottom rotors are opposite to each other; seen from above, the initial rotational directions are such that the top rotor turns anticlockwise (represented by “+”) and the lower rotor turns clockwise (represented by “-”). Figure 3 illustrates the phase angle α , which is the angle between the top and bottom rotor blades, and herein the initial phase angle is $\alpha = 0^\circ$.

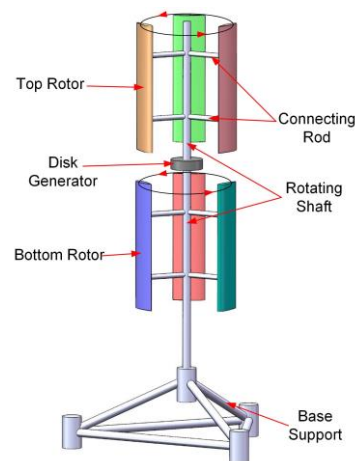


Fig. 1 Structural brief of CR-VAWT

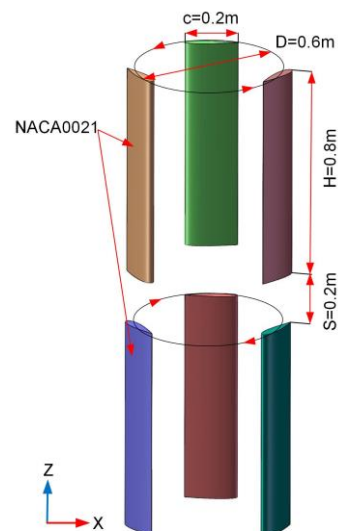


Fig. 2 Initial CR-VAWT schematic

Table 2 Detailed parameters of CR-VAWT

Parameter	Value
Aerofoil	NACA0021
Number of blades (N)	3
Chord length (c)	0.2 m
Turbine diameter (D)	0.6 m
Blade height (H)	0.8 m
Pitch angle (β)	0°
Rotor spacing (S)	0.2 m
Rotational direction (r)	(+, -)
Phase angle (α)	0°

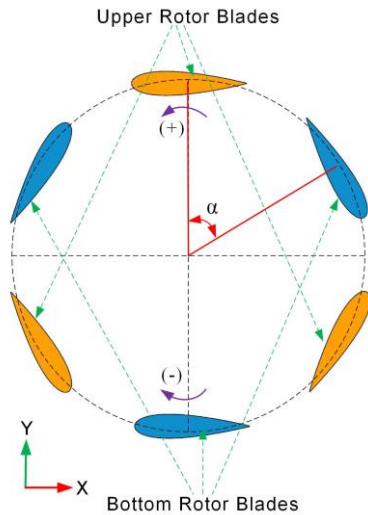


Fig. 3 Phase angle between top and bottom rotors of CR-VAWT

2.2 Computational Domain and Mesh

2.2.1 Computational Domain and Boundary Conditions

Figure 4 illustrates the details of the computational domain, including the stationary and rotational domains. The stationary domain is $15.5D$ long, $6D$ wide and $6D$ high. The rotational domain is a cylindrical body with diameter $1.6D$ and height $1.2H$ (Lei et al., 2017a; Shen et al., 2024).

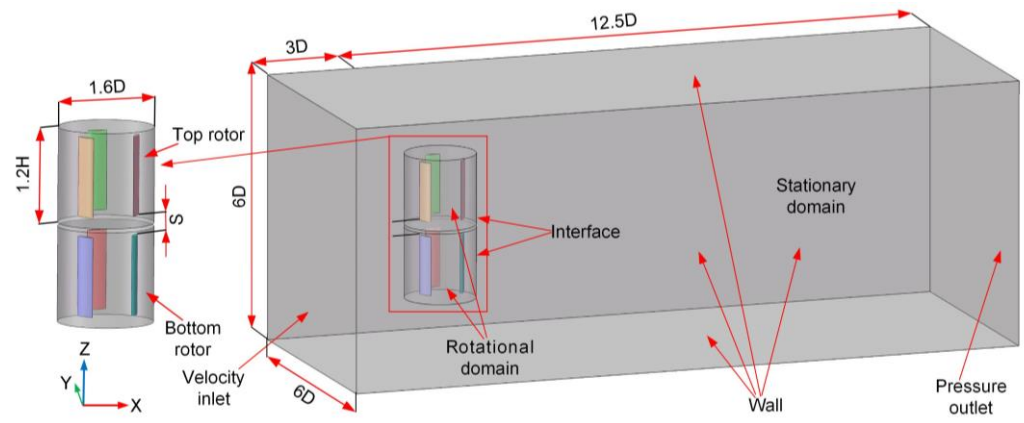


Fig. 4 Dimensions and boundary conditions of computational domain

The inlet wind speed to the stationary domain is $U_0 = 8$ m/s and the turbulence intensity is 5%. The pressure at the pressure outlet is atmospheric. The other faces of the stationary domain are walls. The distances from the centre of the rotational domain to the velocity inlet and pressure outlet are $3D$ and $12.5D$, respectively. The rotational characteristics of the wind-turbine rotor are modelled using the slip mesh technique. The rotational and stationary domain contact surfaces are set to interfaces to allow data exchange at each time-step iteration.

2.2.2 Mesh Division

The Fluent meshing software was used for meshing, and the mesh is shown in detail in Fig. 5. Because the VAWT’s aerodynamic efficiency is the focus of the study, the velocity and pressure distributions of the blades must be captured, and so the mesh near the blades must be refined. Meanwhile, the boundary-layer mesh must be divided in the blade radial direction to precisely capture the pressure and velocity gradient variations close to the blade wall. The precision of the numerical simulation depends on the y^+ value, which also guarantees that $y^+ < 1$ can produce more-accurate computational results (Zamani et al., 2016). The formula for y^+ is

$$y^+ = \frac{y\mu}{\rho u^*} \tag{1}$$

where y is the mesh thickness of the first layer of the boundary layer, μ is the dynamic viscosity, ρ is the fluid density and u^* is the fluid velocity on the blade surface. Herein, y^+ is set to 0.98, which gives $y = 6.818 \times 10^{-5}$ m, 2.97×10^{-3} m for the boundary layer as a whole, and a mesh growth rate of 1.2.

2.3 Governing Equations and Performance Indicators

2.3.1 Governing Equations

Numerical simulations were carried out using the ANSYS Fluent software. The VAWT rotates at high speeds during operation and this causes changes in the flow field, so the operating state of the wind turbine is not constant but rather is always changing with time. Transient simulations can capture these dynamic processes and so are used to investigate the flow characteristics of the VAWT. The linear velocity during operation is always less than Mach 0.3, so the

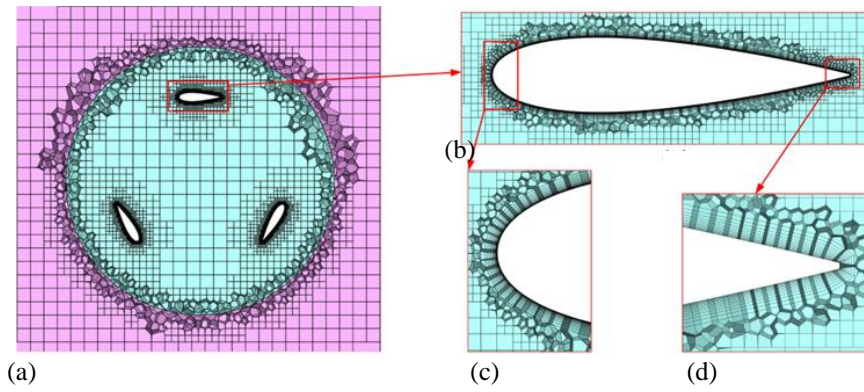


Fig. 5 Mesh density in different regions: (a) rotational domain; (b) boundary layer; (c) leading edge; (d) trailing edge

incompressible unsteady Reynolds-averaged Navier Stokes (URANS) equations (Lei et al., 2017b) are used:

$$\frac{\partial}{\partial x_i}(\bar{u}_i) = 0, \quad (2)$$

$$\rho \frac{\partial}{\partial x_i}(\bar{u}_i) + \rho \frac{\partial}{\partial x_j}(\bar{u}_i \bar{u}_j) = -\frac{\partial \bar{P}}{\partial x_i} + \mu \frac{\partial}{\partial x_i} \left(\frac{\partial \bar{u}_i}{\partial x_i} \right) + \frac{\partial}{\partial x_i}(-\rho \bar{u}'_i \bar{u}'_i), \quad (3)$$

where (\bar{u}_i) is the mean air velocity component, \bar{P} is the mean pressure and $-\rho \bar{u}'_i \bar{u}'_j$ is the particular Reynolds stress tensor associated with the turbulence model.

For accurate numerical simulations, a plausible turbulence model is crucial. The shear stress transport (SST) $k-\omega$ turbulence model is widely used (Chen et al., 2016; Zanforlin & Nishino, 2016; Li et al., 2023) and results in numerical simulations that are in better agreement with experimental results. Therefore, the SST $k-\omega$ turbulence model is chosen, and its control equations are as follows:

$$\frac{\partial}{\partial t}(\rho k) + \frac{\partial}{\partial x_i}(\rho k u_i) = \frac{\partial}{\partial x_j} \left[\Gamma_k \frac{\partial k}{\partial x_j} \right] + G_k - Y_k, \quad (4)$$

$$\frac{\partial}{\partial t}(\rho \omega) + \frac{\partial}{\partial x_j}(\rho \omega u_j) = \frac{\partial}{\partial x_j} \left[\Gamma_\omega \frac{\partial \omega}{\partial x_j} \right] + G_\omega - Y_\omega + D_\omega. \quad (5)$$

where Γ_k and Γ_ω denote the effective diffusivity of k and ω , respectively, G_k and G_ω correspond to k and ω due to the average velocity gradient, respectively, Y_k and Y_ω denote the dissipation of k and ω , respectively, and D_ω is the cross-diffusion term.

The SIMPLEC algorithm was used for the solution, with time discretisation in second-order non-constant implicit format. The pressure and momentum equations were discretised using the second-order windward discretisation format. During the simulation, the residuals were set to 10^{-3} , i.e. a converged solution was obtained when the residuals of all physical quantities were equal to or less than 10^{-3} (Lei et al., 2017a).

2.3.2 Performance Indicators

The main performance indicators of a wind turbine are the torque coefficient C_t and the power coefficient C_p , which are calculated as

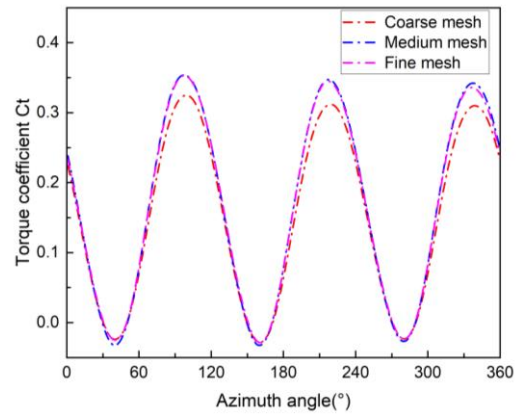


Fig. 6 Instantaneous values of torque coefficient of top rotor on CR-VAWT at three different mesh densities ($\lambda = 1.25$, $U_0 = 8$ m/s)

$$C_t = \frac{T}{\rho U_0^2 H R^2}, \quad (6)$$

$$C_p = \frac{T \omega}{\rho U_0^3 H R}, \quad (7)$$

where T is the torque produced by the wind turbine, ρ is the air density (1.225 kg/m^3), U_0 is the wind speed, H is the blade height, R is the rotating radius of the wind turbine, ω is the rotating angular velocity of the wind turbine blade [rad/s], and λ is the TSR calculated as

$$\lambda = \frac{R\omega}{U_0}. \quad (8)$$

2.4 Verification of Simulation Effectiveness

2.4.1 Mesh Independence

The results of numerical calculations are influenced strongly by the mesh number (Zhang et al., 2023). Therefore, in this study, three meshes were created for simulation, i.e., coarse, medium and fine with 2.51 million, 3.75 million and 4.64 million mesh points, respectively. With $\lambda = 1.25$ and $U_0 = 8$ m/s, the relationship between the instantaneous torque coefficient C_t of the top rotor and the azimuthal angle is shown in Fig. 6 for one full circle of rotation of the CR-VAWT under the three different meshes. As can be seen, the calculation outcomes of the coarse mesh deviate

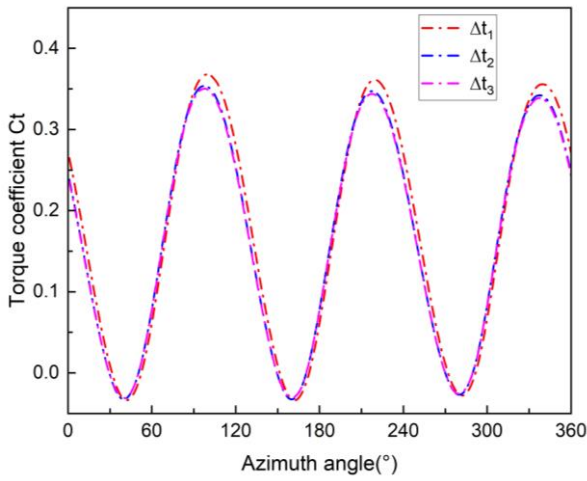


Fig. 7 Instantaneous values of torque coefficient of top rotor on CR-VAWT at three different time steps ($\lambda = 1.25$, $U_0 = 8$ m/s)

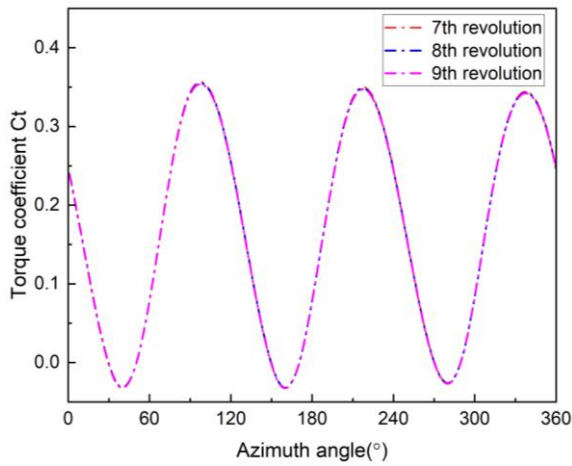


Fig. 8 Instantaneous values of torque coefficient of top rotor on CR-VAWT at three different number of operation revolutions ($\lambda = 1.25$, $U_0 = 8$ m/s)

significantly from those of the medium and fine meshes, whereas the calculation outcomes for the medium and fine meshes are nearly the same. To account for calculation accuracy and cost, the medium-density mesh with a mesh number of 3.7 million was selected for subsequent study.

2.4.2 Time Step

The purpose of time-step validation is to reduce computational resources by using a larger time step while maintaining computational accuracy. Therefore, in this study we set three time steps for validation, i.e. $\Delta t_1 = 0.00026$ s, $\Delta t_2 = 0.00052$ s and $\Delta t_3 = 0.00147$ s, which correspond to the turbine rotating by 0.5° , 1° and 2° , respectively. Figure 7 shows the instantaneous values of the torque coefficient of the top rotor on the CR-VAWT with the three different time steps for $\lambda = 1.25$ and $U_0 = 8$ m/s. As can be seen, the values with Δt_2 and Δt_3 are very close to each other, so $\Delta t_2 = 0.00052$ s was chosen for subsequent study.

Table 3 Detailed parameters of stand-alone VAWT

Parameter	Value
Aerofoil	NACA0021
Number of blades (N)	3
Chord length (c)	0.2 m
Turbine diameter (D)	0.8 m
Blade height (H)	0.8 m

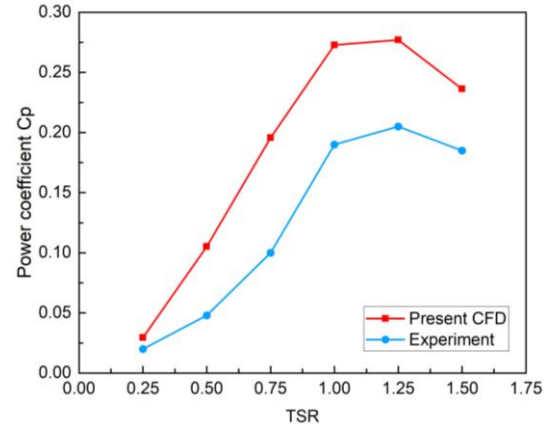


Fig. 9 Comparison between CFD and experimental outcomes under different values of TSR ($U_0 = 8$ m/s)

2.4.3 Number of Operating Revolutions

To enable the wind turbine to reach a steady state of operation and to ensure the precision of the subsequent calculations, a validation of the number of operating revolutions was carried out. Figure 8 shows the instantaneous values of the torque coefficient of the top rotor on the CR-VAWT during three different operating revolutions for $\lambda = 1.25$ and $U_0 = 8$ m/s. As can be seen, the values are very close to each other, indicating that the wind turbine has reached stable operation. Therefore, operations up to the ninth revolution were used for subsequent study.

2.4.4 Simulation Validity

To ensure the dependability of the numerical simulations, their calculated outcomes were compared with the experimental results of [Elkhoury et al. \(2015\)](#); Table 3 lists the detailed parameters of the stand-alone VAWT used in that study. As shown in Fig. 9, for different values of the TSR, the mean values of the power coefficient C_p of the VAWT as obtained by the present CFD agree with the trend of the original experimental results. However, because we simplify the components of the rotating shaft and connecting rod, the simulation results are larger than the experimental ones, but the resulting error is acceptable.

3. OPTIMISED DESIGN WITH TAGUCHI'S METHOD

3.1 Optimised Objective Variable

This research uses Taguchi's method to optimise the parameters of the CR-VAWT, aiming to enhance its wind

Table 4 CR-VAWT design factors and levels

Design factor	Parameter	Symbol	Levels			
			1	2	3	4
A	Rotor spacing	S [m]	0.2	0.4	0.6	0.8
B	Diameter-to-height ratio	D/H [-]	0.75	1	1.25	1.5
C	Phase angle	α [°]	0	30	60	90
D	Rotational direction	r [-]	(+, -)	(-, +)	-	-

energy efficiency. The main principle of Taguchi’s method is to derive the optimum solution for multifactor design by combining orthogonal tables with signal-to-noise (S/N) ratios, making it possible to minimise the quality loss of the project. The objective variable optimised herein is the average power coefficient of the top and bottom rotors of the CR-VAWT, which is expressed as

$$Cp_{avg} = \frac{Cp_1 + Cp_2}{2}, \tag{9}$$

where Cp_1 and Cp_2 are the power coefficients of the top and bottom rotors of the CR-VAWT, respectively. To characterise the effect of the difference between the target variable and the target value on system performance, we introduce a mass loss function, which has different forms depending on the objective value. Herein, the objective is to maximise the mean power coefficient of the CR-VAWT, so the mass loss function is expressed as

$$L(y) = \frac{K}{y^2}, \tag{10}$$

where y is the test value corresponding to Cp_{avg} herein, and K is the mass loss coefficient.

3.2 Design Factors and Orthogonal Tables

We consider the effects of both arrangement and structural factors on the aerodynamic efficiency of the CR-VAWT, i.e. the mounting spacing of the top and bottom rotors (S), the phase angle (α), the rotational direction (r) and the diameter-to-height ratio (D/H), which is the ratio of rotor diameter to blade height; keeping the blade height constant, D/H is varied by changing the rotor diameter. Four design levels are selected for S , α and D/H , and two

are selected for r . Table 4 gives the design factors, and Table 5 gives the L16 ($4^3 \times 2^1$) mixed orthogonal table.

Figure 9 shows that Cp of the stand-alone VAWT is maximum when the TSR is 1.25, so all the simulation experiments based on the L16 hybrid orthogonal table were conducted at this TSR. The findings of the simulation experiments are used to obtain the optimal design parameters that maximise Cp_{avg} of the CR-VAWT. The signal-to-noise ratio (S/N) is introduced to analyse how the design parameters affect Cp_{avg} . In Taguchi’s method, S/N is a quality metric used to measure the impact of each design factor on mass loss. The quality loss function is usually expressed using S/N , and there are three types: (i) smaller S/N is better, (ii) larger S/N is better and (iii) nominal S/N is better. Herein, the larger the value of Cp_{avg} of the CR-VAWT, the better; therefore, larger S/N is used to select the optimal design parameter with the following expression:

$$S/N = -10 \log\left(\frac{1}{n} \sum_{i=1}^n \frac{1}{y_i^2}\right), \tag{11}$$

where n is the number of simulation experiments ($n = 1$ herein) and y_i is the mean power coefficient Cp_{avg} of the CR-VAWT.

4. RESULTS AND DISCUSSION

4.1 Optimised Results

Three-dimensional simulation experiments were performed based on the L16 hybrid orthogonal table in Table 5. The results are reported in Table 6, with S/N calculated in each case according to Eq. (11). The impact

Table 5 L16 ($4^3 \times 2^1$) mixed orthogonal table

Cases	Factors (coded)				Factors (uncoded)			
	A	B	C	D	S [m]	D/H [-]	α [°]	r [-]
1	1	1	1	1	0.2	0.75	0°	(+,-)
2	1	2	2	1	0.2	1	30°	(+,-)
3	1	3	3	2	0.2	1.25	60°	(-,+)
4	1	4	4	2	0.2	1.5	90°	(-,+)
5	2	1	2	2	0.4	0.75	30°	(-,+)
6	2	2	1	2	0.4	1	0°	(-,+)
7	2	3	4	1	0.4	1.25	90°	(+,-)
8	2	4	3	1	0.4	1.5	60°	(+,-)
9	3	1	3	1	0.6	0.75	60°	(+,-)
10	3	2	4	1	0.6	1	90°	(+,-)
11	3	3	1	2	0.6	1.25	0°	(-,+)
12	3	4	2	2	0.6	1.5	30°	(-,+)
13	4	1	4	2	0.8	0.75	90°	(-,+)
14	4	2	3	2	0.8	1	60°	(-,+)
15	4	3	2	1	0.8	1.25	30°	(+,-)
16	4	4	1	1	0.8	1.5	0°	(+,-)

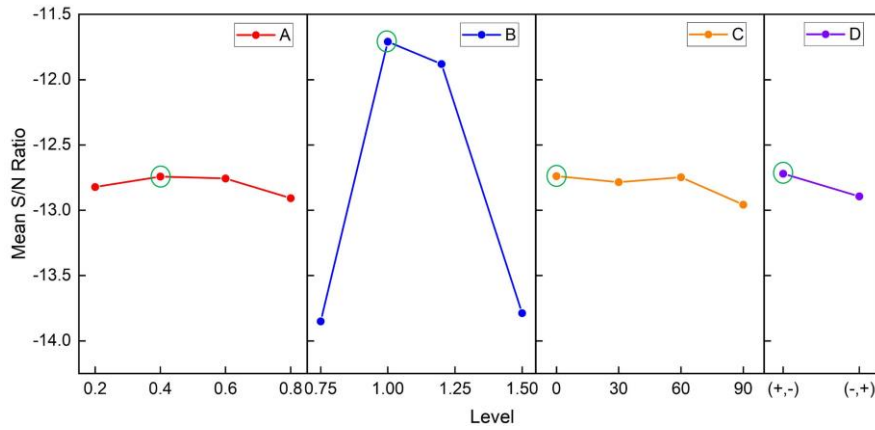


Fig. 10 Mean S/N ratio of each factor at each level

Table 6 Results of orthogonal experiments ($\lambda = 1.25, U_0 = 8 \text{ m/s}$)

Cases	Cp_1	Cp_2	Cp_{avg}	S/N
1	0.2065	0.2067	0.2066	-13.6982
2	0.2612	0.2605	0.2609	-11.6705
3	0.2547	0.2538	0.2542	-11.8956
4	0.2005	0.1975	0.1990	-14.0222
5	0.2012	0.2069	0.2041	-13.8039
6	0.2615	0.2607	0.2611	-11.6650
7	0.2573	0.2593	0.2583	-11.7577
8	0.2060	0.2052	0.2056	-13.7398
9	0.2091	0.2090	0.2091	-13.5936
10	0.2607	0.2569	0.2588	-11.7412
11	0.2524	0.2529	0.2527	-11.9479
12	0.2031	0.2078	0.2055	-13.7459
13	0.1947	0.1905	0.1926	-14.3080
14	0.2589	0.2576	0.2582	-11.7599
15	0.2548	0.2522	0.2535	-11.9201
16	0.2079	0.2079	0.2079	-13.6429

of each factor on the power coefficient is investigated by performing a range analysis of S/N (Song et al., 2016). The average S/N of factor T at level t is represented as

$$(\overline{S/N})_{Factor=T}^{level=t} = \frac{1}{P} \sum_{Q=1}^P [(S/N)_{Factor=T}^{level=t}]_Q, \quad (12)$$

where P denotes the number of occurrences of factor T at level t , and Q denotes the Q th occurrence. At level 1, the S/N of factor A is $-13.6982, -11.6705, -11.8956$ and -14.0222 , and its $(\overline{S/N})$ is $(\overline{S/N})_{Factor=T}^{level=t} = 1/4(-13.6982 - 11.6705 - 11.8956 - 14.0222) = -12.8217$. $(\overline{S/N})$ for each factor was calculated as presented in Fig. 10, where the horizontal axis represents the level values of the factors and the vertical axis represents $(\overline{S/N})$. As can be seen, $(\overline{S/N})$ is maximum when $S = 0.4 \text{ m}, D/H = 1, \alpha = 0^\circ$ and $r = (+, -)$. The larger $(\overline{S/N})$, the larger the mean power coefficient of the CR-VAWT, so the optimal design solution is derived as $A_2B_2C_1D_1$, which corresponds to the optimal design parameters of $S = 0.4 \text{ m}, D/H = 1, \alpha = 0^\circ$ and $r = (+, -)$.

To derive the extent of the effect of each design factor on Cp of the CR-VAWT, a range study of $(\overline{S/N})$ was conducted. The weight (Ei) of each design factor on Cp is

the difference between the maximum and minimum $(\overline{S/N})$ of that factor, i.e.

$$Ei = \max\{(\overline{S/N})_{Factor=T}^{level=1}, \dots, (\overline{S/N})_{Factor=T}^{level=P}\} - \min\{(\overline{S/N})_{Factor=T}^{level=1}, \dots, (\overline{S/N})_{Factor=T}^{level=P}\}, \quad (13)$$

where P is the number of levels of factor T , which is four for factors A, B and C and two for factor D.

The extent to which each factor affects Cp of the CR-VAWT was calculated by Eq. (13) as shown in Fig. 11, where the horizontal coordinate denotes the factor and the vertical coordinate denotes the weight Ei . Figure 11 shows that D/H has the greatest effect (81.21%) on Cp , followed by α (7.37%) and then r (5.83%), with S having the smallest effect (5.59%). This shows that selecting D/H correctly is important for the power performance of a CR-VAWT, whereas α, r and S have less effect.

4.2 Power Performance of Optimum CR-VAWT and Stand-alone VAWT

We calculate the optimum CR-VAWT and the stand-alone VAWT at various low TSRs. The variation of the mean power coefficient Cp_{avg} of the two rotors of the

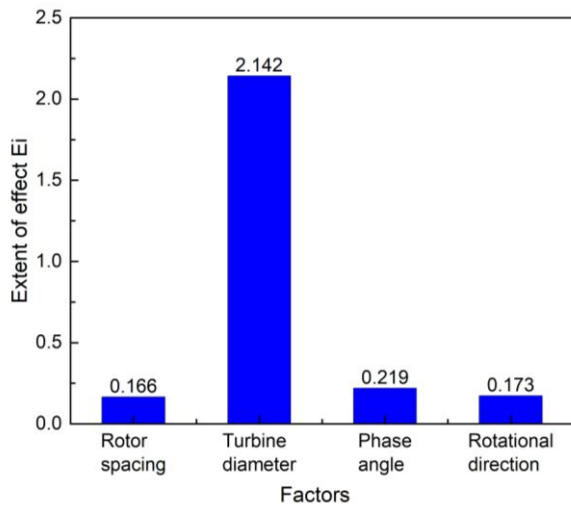


Fig. 11 Extent of effect of each design factor on $C_{p_{avg}}$

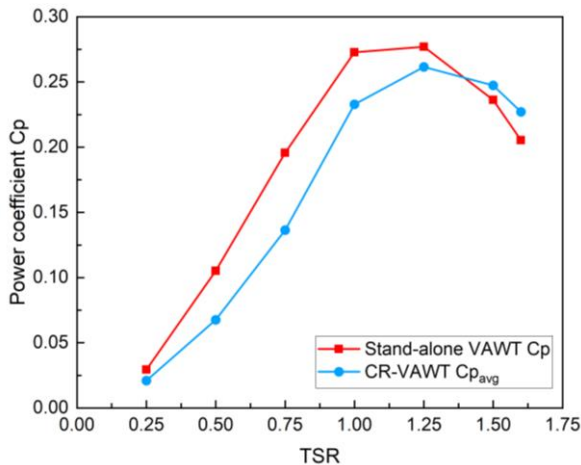


Fig. 12 Variation curve of power coefficient with TSR ($U_0 = 8 \text{ m/s}$)

optimum CR-VAWT and the power coefficient C_p of the stand-alone VAWT is shown in Fig. 12.

When the TSR less than 1.25, the average power coefficient $C_{p_{avg}}$ of the optimum CR-VAWT optimised by Taguchi’s method is smaller than that of the stand-alone VAWT, but this difference decreases with increasing TSR. When the TSR is increased to 1.25, both the optimal CR-VAWT and the stand-alone VAWT achieve their peak power coefficient. At this time, $C_{p_{avg}}$ of the optimum CR-VAWT is 0.2615, which is 94.4% of that of the stand-alone VAWT. As the TSR continues to be increased, the power performance of the optimum CR-VAWT gradually outperforms that of the stand-alone VAWT. When the TSR is 1.5, $C_{p_{avg}}$ of the optimum CR-VAWT is 0.2474, which is a 4.7% improvement relative to the stand-alone VAWT. When the TSR is increased to 1.6, $C_{p_{avg}}$ of the optimum CR-VAWT is improved by 10.6%.

The dimensional parameters of the optimum CR-VAWT (top rotor) and the stand-alone VAWT are identical, so to further analyse the difference in power coefficients between the optimum CR-VAWT and the stand-alone VAWT, their instantaneous power

coefficients were compared at TSRs of 0.75, 1.25, 1.5 and 1.6, as shown in Fig. 13. At these TSRs, the azimuthal angle at which the instantaneous power coefficient of the top rotor peaks is advanced compared to that of the stand-alone VAWT, mainly because the top and bottom rotors overlap at azimuthal angles of 120° , 240° and 360° . Therefore, the tip vortices of the top and bottom rotors interact with each other, resulting in reduced power performance.

For $\lambda = 0.75$, the instantaneous power coefficient of the top rotor is smaller than that of the stand-alone VAWT at almost all azimuths, and the average power coefficient of the top rotor (C_{p1}) is 0.1363, which is only 69.7% of that of the stand-alone VAWT. For $\lambda = 1.25$, the maximum instantaneous power coefficient of the top rotor is 0.5039, which already exceeds that of the stand-alone VAWT. However, the average power coefficient remains less than that of the stand-alone VAWT. For $\lambda = 1.5$ or 1.6, the maximum instantaneous and average power coefficients of the top rotor are higher than those of the stand-alone VAWT, and the overall power performance is better than that of the stand-alone VAWT.

Figure 14 shows time series of the torques of the optimum CR-VAWT and the stand-alone VAWT for $\lambda = 1.25$. The optimum CR-VAWT has the same torque trend for both the top and bottom rotors. However, because the rotational direction is reversed, the torques transmitted to the rotor base support through the rotating shaft are almost equal in amount and opposite in direction and so cancel out, resulting in less total torque for the optimum CR-VAWT. The largest total torque of the optimal CR-VAWT and the stand-alone VAWT is 0.2209 N m and 3.6597 N m, respectively. The CR-VAWT has only 6% of the largest torque of the stand-alone VAWT, so the total torque transmitted to the rotor base support is reduced, which results in better structural stability of the optimum CR-VAWT. Also, the damage to the rotor base support is less, thereby prolonging its service life.

4.3 Pressure-field analysis of optimum CR-VAWT and stand-alone VAWT

As shown in Fig. 15. For $\lambda = 1.25$ and $\alpha = 30^\circ$, the areas of negative pressure for blades 1 and 3 of the stand-alone VAWT are larger, indicating a larger pressure differential on both sides of the blades, and at this time the stand-alone VAWT has a larger power coefficient. At $\alpha = 60^\circ$ or 90° , the negative-pressure region on the suction surface of blade 1 of the top rotor increases compared to the stand-alone VAWT. The pressure differential on the surface of blade 1 then increases, and at this time the top-rotor power coefficient is larger. At $\alpha = 120^\circ$, the negative-pressure region of the suction surface of blade 1 of the top rotor is decreased compared to the stand-alone VAWT, so the power coefficient of the top rotor is smaller. At $\alpha = 150^\circ$, blades 1 and 2 of the stand-alone VAWT have a larger pressure differential on both sides, so its power coefficient is larger. The results for the stand-alone VAWT by pressure cloud mapping are consistent with Fig. 14(b). In conclusion, the blades of the stand-alone VAWT have a slightly better overall pressure differential than does the top rotor of the optimum CR-VAWT and so have better power performance.

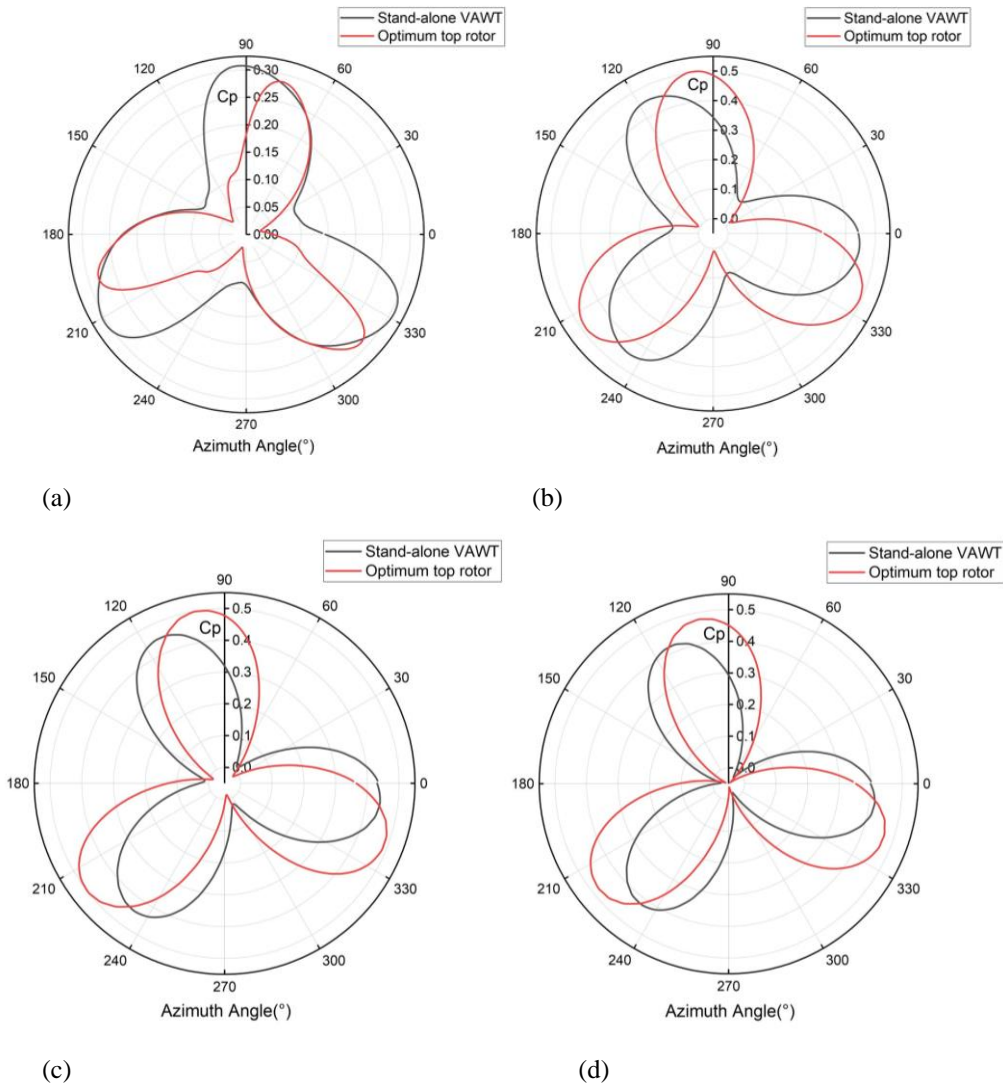


Fig. 13 Variation of instantaneous power coefficient with azimuth angle for $\lambda =$ (a) 0.75, (b) 1.25, (c) 1.5, and (d) 1.6 ($U_0 = 8$ m/s)

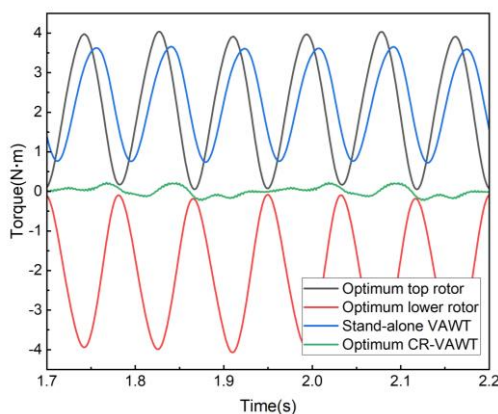


Fig. 14 Comparison of torques of optimum CR-VAWT and stand-alone VAWT ($\lambda = 1.25$, $U_0 = 8$ m/s)

For $\lambda = 1.5$ and $\alpha = 30^\circ$, the pressure differential on both sides of blade 2 of the stand-alone VAWT is larger, resulting in a larger power coefficient. At $\alpha = 60^\circ$ or 90° ,

rotor blades 1, 2 and 3 of the optimum CR-VAWT have a greater pressure differential on both sides compared to the stand-alone VAWT, resulting in a larger power coefficient of the top rotor. At $\alpha = 120^\circ$ or 150° , the negative-pressure region of blade 1 of the stand-alone VAWT increases slightly, and the pressure differential on both sides of blade 1 is larger. At this time, the power coefficient of the stand-alone VAWT is larger. The top rotor of the optimum CR-VAWT has a larger overall pressure differential on both sides of each blade compared to the stand-alone VAWT, so it has better power performance at this TSR.

5. CONCLUSION

In the present study to derive an optimal CR-VAWT, CFD was combined with Taguchi's method to systematically optimise the four main parameters affecting the configuration of a three-blade H-type CR-VAWT, i.e. rotor pitch (S), diameter-to-height ratio (D/H), phase angle (α) and rotational direction (r). The aerodynamic efficiency of the optimum CR-VAWT was

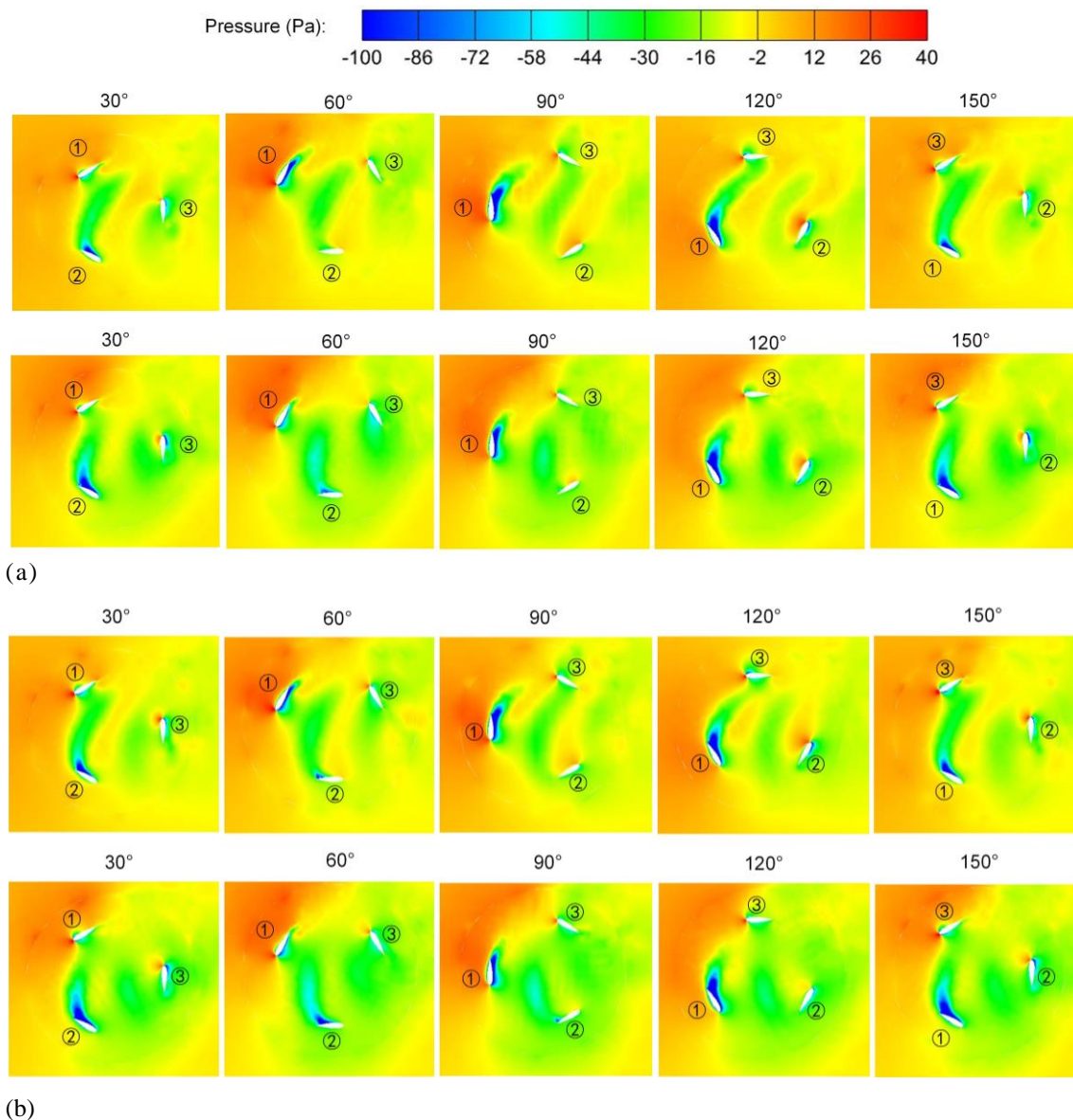


Fig. 15 Pressure clouds at different azimuthal angles for top rotor of optimum CR-VAWT (upper row) and stand-alone VAWT (lower row) for $\lambda =$ (a) 1.25 and (b) 1.5 ($U_0 = 8$ m/s)

compared with that of a stand-alone VAWT at low TSR, and the following main conclusions were drawn from this research.

1) The optimum design of the CR-VAWT as optimised using Taguchi's method is $A_2B_2C_1D_1$, corresponding to the optimal configuration parameters of $S = 0.4$ m, $D/H = 1$, $\alpha = 0^\circ$ and $r = (+, -)$.

2) The extent of the effect of each factor on the power performance of the CR-VAWT is as follows. D/H has the greatest effect (81.21%), followed by α (7.37%) and then r (5.83%), with S having the least effect (5.59%).

3) Compared to the stand-alone VAWT, the average power coefficient of the optimum CR-VAWT is significantly smaller when the TSR is less than 1.25. The power performance of the optimum CR-VAWT gradually prevails as the TSR is increased. At a TSR of 1.6, the optimum CR-VAWT has an improvement in its average power factor of 10.6% over the stand-alone VAWT.

4) The top and bottom rotors of the optimum CR-VAWT rotate in opposite directions, so the generated torques are cancelled out. Its maximum total torque is 0.2209 N m, which is only 6% of that of the stand-alone VAWT. The torque transmitted to the rotor base support is greatly reduced, which makes the optimum CR-VAWT stable.

ACKNOWLEDGEMENTS

This study was funded by the National Natural Science Foundation of China (No. 52205286), the Natural Science Foundation of Xinjiang Uygur Autonomous Region (No. 2022D01C33) and the Graduate Research Innovation Project of Xinjiang Uygur Autonomous Region (No. XJ2024G091).

CONFLICT OF INTEREST

The authors have no conflicts of interests to disclose.

AUTHORS CONTRIBUTION

Zhikai Zhao: Methodology, Conceptualization, Validation, Software, Writing – original draft, Data curation, Formal analysis; **Kun Chen:** Project administration, Writing – review & editing, Funding acquisition, Resources; **Qi Wang:** Project administration, Formal analysis; **Tao Su:** Investigation, Formal analysis; **Hongyi Hu:** Investigation, Formal analysis.

REFERENCES

- Chen, J., Chen, L., Xu, H., Yang, H., Ye, C., & Liu, D. (2016). Performance improvement of a vertical axis wind turbine by comprehensive assessment of an airfoil family. *Energy*, *114*, 318-331. <http://dx.doi.org/10.1016/j.energy.2016.08.005>
- Chen, W. H., Chen, C. Y., Huang, C. Y., & Hwang, C. J. (2017). Power output analysis and optimization of two straight-bladed vertical-axis wind turbines. *Applied Energy*, *185*, 223-232. <http://dx.doi.org/10.1016/j.apenergy.2016.10.076>
- Didane, D. H., Rosly, N., Zulkafli, M. F., & Shamsudin, S. S. (2018). Performance evaluation of a novel vertical axis wind turbine with coaxial contra-rotating concept. *Renewable Energy*, *115*, 353-361. <http://dx.doi.org/10.1016/j.renene.2017.08.070>
- Didane, D. H., Rosly, N., Zulkafli, M. F., & Shamsudin, S. S. (2019). Numerical investigation of a novel contra-rotating vertical axis wind turbine. *Sustainable Energy Technologies and Assessments*, *31*, 43-53. <http://dx.doi.org/10.1016/j.seta.2018.11.006>
- Dong, Z., Wang, X., Zhu, R., Dong, X., & Ai, X. (2022). Improving the accuracy of wind speed statistical analysis and wind energy utilization in the Ningxia Autonomous Region, China. *Applied Energy*, *320*. <http://dx.doi.org/10.1016/j.apenergy.2022.119256>
- Elkhoury, M., Kiwata, T., & Aoun, E. (2015). Experimental and numerical investigation of a three-dimensional vertical-axis wind turbine with variable-pitch. *Journal of Wind Engineering and Industrial Aerodynamics*, *139*, 111-123. <http://dx.doi.org/10.1016/j.jweia.2015.01.004>
- Farzadi, R., & Bazargan, M. (2023). 3D numerical simulation of the Darrieus vertical axis wind turbine with J-type and straight blades under various operating conditions including self-starting mode. *Energy*, *278*. <http://dx.doi.org/10.1016/j.energy.2023.128040>
- Hassanpour, M., & Azadani, L. N. (2021). Aerodynamic optimization of the configuration of a pair of vertical axis wind turbines. *Energy Conversion and Management*, *238*. <http://dx.doi.org/10.1016/j.enconman.2021.114069>
- Lee, Y. T., & Lim, H. C. (2015). Numerical study of the aerodynamic performance of a 500 W Darrieus-type vertical-axis wind turbine. *Renewable Energy*, *83*, 407-415. <http://dx.doi.org/10.1016/j.renene.2015.04.043>
- Lei, H., Zhou, D., Bao, Y., Li, Y., & Han, Z. (2017a). Three-dimensional Improved Delayed Detached Eddy Simulation of a two-bladed vertical axis wind turbine. *Energy Conversion and Management*, *133*, 235-248. <http://dx.doi.org/10.1016/j.enconman.2016.11.067>
- Lei, H., Zhou, D., Bao, Y., Chen, C., Ma, N., & Han, Z. (2017b). Numerical simulations of the unsteady aerodynamics of a floating vertical axis wind turbine in surge motion. *Energy*, *127*, 1-17. <http://dx.doi.org/10.1016/j.energy.2017.03.087>
- Li, Y., Yang, S., Feng, F., & Tagawa, K. (2023). A review on numerical simulation based on CFD technology of aerodynamic characteristics of straight-bladed vertical axis wind turbines. *Energy Reports*, *9*, 4360-4379. <http://dx.doi.org/10.1016/j.egyr.2023.03.082>
- Liao, C. N., & Kao, H. P. (2010). Supplier selection model using Taguchi loss function, analytical hierarchy process and multi-choice goal programming. *Computers & Industrial Engineering*, *58*(4), 571-577. <http://dx.doi.org/10.1016/j.cie.2009.12.004>
- Malicki, L., Malecha, Z., Baran, B., & Juszko, R. (2024). Numerical investigation of a novel type of rotor working in a palisade configuration. *Energies*, *17*(13). <http://dx.doi.org/10.3390/en17133093>
- Peng, H. Y., Liu, H. J., & Yang, J. H. (2021). A review on the wake aerodynamics of H-rotor vertical axis wind turbines. *Energy*, *232*. <http://dx.doi.org/10.1016/j.energy.2021.121003>
- Poguluri, S. K., Lee, H., & Bae, Y. H. (2021). An investigation on the aerodynamic performance of a co-axial contra-rotating vertical-axis wind turbine. *Energy*, *219*. <http://dx.doi.org/10.1016/j.energy.2020.119547>
- Radhakrishnan, J., Sridhar, S., Zuber, M., Ng, E. Y. K., & B, S. S. (2023). Design optimization of a Contra-Rotating VAWT: A comprehensive study using Taguchi method and CFD. *Energy Conversion and Management*, *298*. <http://dx.doi.org/10.1016/j.enconman.2023.117766>
- Sanaye, S., & Farvizi, A. (2024). Optimizing a vertical axis wind turbine with helical blades: Application of 3D CFD and Taguchi method. *Energy Reports*, *12*, 2527-2547. <http://dx.doi.org/10.1016/j.egyr.2024.08.059>
- Shen, Z., Gong, S., Xie, G., Lu, H., & Guo, W. (2024). Investigation of the effect of critical structural parameters on the aerodynamic performance of the double darrieus vertical axis wind turbine. *Energy*, *290*. <http://dx.doi.org/10.1016/j.energy.2023.130156>
- Song, L., Fu, S., Dai, S., Zhang, M., & Chen, Y. (2016). Distribution of drag force coefficient along a flexible riser undergoing VIV in sheared flow. *Ocean Engineering*, *126*, 1-11. <http://dx.doi.org/10.1016/j.oceaneng.2016.08.022>
- Sun, S. Y., Liu, H. J., & Peng, H. Y. (2023). Power

- performance and self-starting features of H-rotor and helical vertical axis wind turbines with different airfoils in turbulence. *Energy Conversion and Management*, 292. <http://dx.doi.org/10.1016/j.enconman.2023.117405>
- Wang, Y., Shen, S., Li, G., Huang, D., & Zheng, Z. (2018). Investigation on aerodynamic performance of vertical axis wind turbine with different series airfoil shapes. *Renewable Energy*, 126, 801-818. <http://dx.doi.org/10.1016/j.renene.2018.02.095>
- Zamani, M., Maghrebi, M. J., & Varedi, S. R. (2016). Starting torque improvement using J-shaped straight-bladed Darrieus vertical axis wind turbine by means of numerical simulation. *Renewable Energy*, 95, 109-126. <http://dx.doi.org/10.1016/j.renene.2016.03.069>
- Zanforlin, S., & Nishino, T. (2016). Fluid dynamic mechanisms of enhanced power generation by closely spaced vertical axis wind turbines. *Renewable Energy*, 99, 1213-1226. <http://dx.doi.org/10.1016/j.renene.2016.08.015>
- Zhang, Q., Bashir, M., Miao, W., Liu, Q., Li, C., Yue, M., & Wang, P. (2023). Aerodynamic analysis of a novel pitch control strategy and parameter combination for vertical axis wind turbines. *Renewable Energy*, 216. <http://dx.doi.org/10.1016/j.renene.2023.119089>
- Zhang, T., Wang, Z., Huang, W., Ingham, D., Ma, L., & Pourkashanian, M. (2020). A numerical study on choosing the best configuration of the blade for vertical axis wind turbines. *Journal of Wind Engineering and Industrial Aerodynamics*, 201. <http://dx.doi.org/10.1016/j.jweia.2020.104162>
- Zhang, Y., Li, Q. a., Zhu, X., Song, X., Cai, C., Zhou, T., Guo, Z. (2022). Effect of the bionic blade on the flow field of a straight-bladed vertical axis wind turbine. *Energy*, 258. <http://dx.doi.org/10.1016/j.energy.2022.124834>
- Zheng, P., Zhang, H., Zhang, Z., Salman, W., & Abdelrahman, M. (2024). Parameter optimization method of contra-rotating vertical axis wind turbine: Based on numerical simulation and response surface. *Journal of Cleaner Production*, 435. <http://dx.doi.org/10.1016/j.jclepro.2023.140475>
- Zhu, H., Hao, W., Li, C., Luo, S., Liu, Q., & Gao, C. (2021). Effect of geometric parameters of Gurney flap on performance enhancement of straight-bladed vertical axis wind turbine. *Renewable Energy*, 165, 464-480. <http://dx.doi.org/10.1016/j.renene.2020.11.027>